ACS APPLIED MATERIALS & INTERFACES

www.acsami.org

Research Article

# A Novel Approach for Colloidal Lithography: From Dry Particle Assembly to High-Throughput Nanofabrication

Sivan Tzadka, Carlos Ureña Martin, Esti Toledo, Abed Al Kader Yassin, Ashish Pandey, Guillaume Le Saux, Angel Porgador, and Mark Schvartzman*

Cite This: *ACS Appl. Mater. Interfaces* 2024, 16, 17846−17856

Read Online

ACCESS | Metrics & More | Article Recommendations | Supporting Information

**ABSTRACT:** We introduce a novel approach for colloidal lithography based on the dry particle assembly into a dense monolayer on an elastomer, followed by mechanical transfer to a substrate of any material and curvature. This method can be implemented either manually or automatically and it produces large area patterns with the quality obtained by the state-of-the-art colloidal lithography at a very high throughput. We first demonstrated the fabrication of nanopatterns with a periodicity ranging between 200 nm and 2 $\mu$m. We then demonstrated two nanotechnological applications of this approach. The first one is antireflective structures, fabricated on silicon and sapphire, with different geometries including arrays of bumps and holes and adjusted for different spectral ranges. The second one is smart 3D nanostructures for mechanostimulation of T cells that are used for their effective proliferation, with potential application in cancer immunotherapy. This new approach unleashes the potential of bottom-up nanofabrication and paves the way for nanoscale devices and systems in numerous applications.

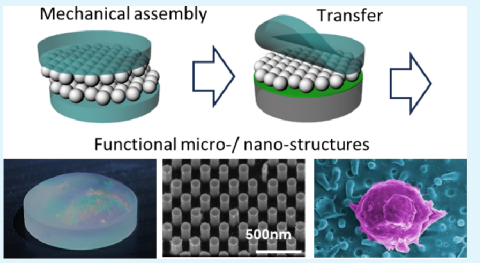


**KEYWORDS:** *self-assembly, colloidal lithography, antireflective structures, nanoparticles, sapphire, T cells*



## INTRODUCTION

For several decades, colloidal lithography has been considered as a promising bottom-up approach for producing micro/nanoscale patterns. Its most significant advantage is undoubtedly its simplicity and cost-effectiveness. It requires minimal equipment and is based on micro/nanoscale spherical particles that are commercially available or, alternatively, can be synthesized using relatively easy and well-established protocols.[1−3] Importantly, colloidal lithography is often described in the literature as a way for producing ordered periodic patterns. However, it is, in fact, a kinetically controlled assembly process into polycrystalline 2D structure with short-range order, which comprises relatively small crystalline domains separated by pronounced grain boundaries.[4,5] On the other hand, many nanotechnological applications do not necessarily require patterns with long-range order and can therefore be successfully implemented using colloidal lithography.[6,7] Numerous examples of such applications include, but are not limited to, functional nanoscale structures in photonics,[8−10] plasmonics,[11,12] biology,[13] and renewable energy.[14,15]

Despite significant developments in colloidal lithography and its applications, its usage is still mostly limited to the world of academic research, and commercial potential is still far from being realized for two main reasons. The first reason refers to the particle monolayer's insufficient quality and packing density. It must be noted that while the scientific reports on the assembly of colloidal particles typically show images of small areas covered with highly ordered and closely packed monolayers of particles, they ignore commonly obtained defects—empty areas and areas with double- and multilayers. The size and abundance of these defects, in turn, greatly depend on the assembly method.[16,17] Spin coating, which is likely the easiest way to assemble colloidal particles, would always produce a substantial amount of defects, up to tens of percents of the total area.[18] Dip coating,[19] solvent evaporation,[20] and Langmuir−Blodgett[21] assembly produce colloidal monolayers with improved quality, yet they cannot completely prevent defects. Other approaches for self-assembly, such as drop casting,[22] evaporation in cell,[23] drag coating,[24] and assembly at the interface between two liquids,[25] also produce high density of defects, including areas uncovered with particles, as well as the area of particle aggregations into multilayer.

The negative impact of defects on the pattern functionality can be illustrated in antireflective 'moth-eye' structures.[26] Colloidal lithography is an appealing method for the fabrication of moth-eye structures;[27,28] however, the light scattering from the defects prevents the antireflective structures from reaching their optimal antireflective performance

Received: December 11, 2023
Revised: March 18, 2024
Accepted: March 18, 2024
Published: March 29, 2024

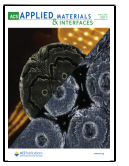

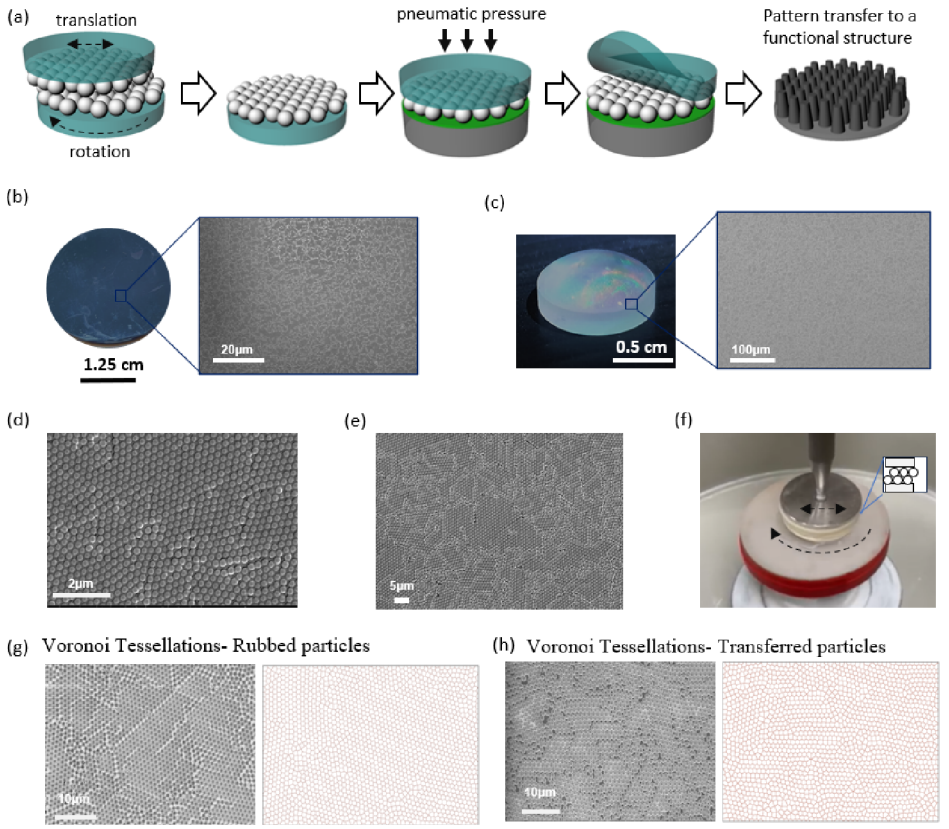


**Figure 1.** (a) Schematic process flow of the dry assembly followed by a pattern transfer to a functional; micro/nanostructure. (b) A monolayer of 200 nm polystyrene spheres transferred on to flat silicon surface. (c) A monolayer of 1 $\mu$m polystyrene spheres transferred to glass lens. (d) and (e) High-magnification SEM images of 200 nm and 1 $\mu$m transferred particles monolayer. (f) Rubbing of two PDMS surfaces using an automated machine. (g) and (h) SEM images and Voronoi Tessellations of 1 $\mu$m polystyrene spheres before and after the transfer, respectively.

predicted by theory.[29,30] The second reason that impedes the commercialization of colloidal lithography is the low throughput of assembly methods. For instance, it typically takes a few hours to cover a few centimeters of surface with a particle monolayer by the Langmuir−Blodgett method, and such time scales make this process impractical for scalable fabrication of optical surfaces.

Colloidal lithography has traditionally been viewed as a method involving particle assembly from liquid suspension onto solid surfaces, driven by meniscus drying at the liquid−solid−air interface. Yet, particles can also be organized into a monolayer by 'dry assembly', in which the particle powder is rubbed between two surfaces. Dry assembly was demonstrated decades ago.[31,32] However, it has not been popularized, probably due to the relatively low packing density and order of the obtained monolayer, as compared to those produced by Langmuir−Blodgett or dip-coating methods. The formation of a monolayer with the high density and uniform orientation of crystalline domains was reported later by rubbing between two elastomer surfaces, in which the aggregation of particles is prevented since the elastomer−particle adhesion is stronger than the interaction between the particles.[33] This approach has opened a pathway to scalable, high-quality colloidal lithography. However, it has been limited to producing monolayers only on elastomer surfaces, which substantially restricts the applications of this promising fabrication approach.

Here, we demonstrate a new approach for colloidal lithography based on the dry particle assembly into a dense monolayer on the elastomer and the monolayer transfer to a target substrate, which can be either flat or curved and be made of any material. The pattern formed by the monolayer is then further transferred to the substrate to produce a functional micro-/nanostructure (Figure 1a). Using this method, we demonstrated the fabrication of structures with periodicity in the range of 200 nm to 2 $\mu$m. We also demonstrated that this fabrication method could be used in a diverse range of applications. In this paper, we focused on two applications: the production of optical structures with antireflective functionality and bioactive topographical structures for the activation and proliferation of human T cells−white blood lymphocytes that are exploited in novel immunotherapy against cancer. Overall, this work produces a new, scalable, and highly effective nanofabrication approach with numerous nanotechnological applications.

## RESULTS AND DISCUSSION

The first step of the fabrication process is the mechanical rubbing of nanoparticles between two elastomer substrates. Notably, previously reported unidirectional rubbing was shown to align the orientation of crystalline domains in the monolayer.[33] In contrast to that method, here we focused on applications that are insensitive to the orientation of the crystalline domains, which allowed us to probe different ways to move the surface, including uniaxial rotation of both elastomer surfaces to the same or opposite directions and linear motions of the two elastomers at various directions with respect to each other. We found that monolayers with the highest quality and packing are achieved while the lower


https://doi.org/10.1021/acsami.3c18554
ACS Appl. Mater. Interfaces 2024, 16, 17846−17856

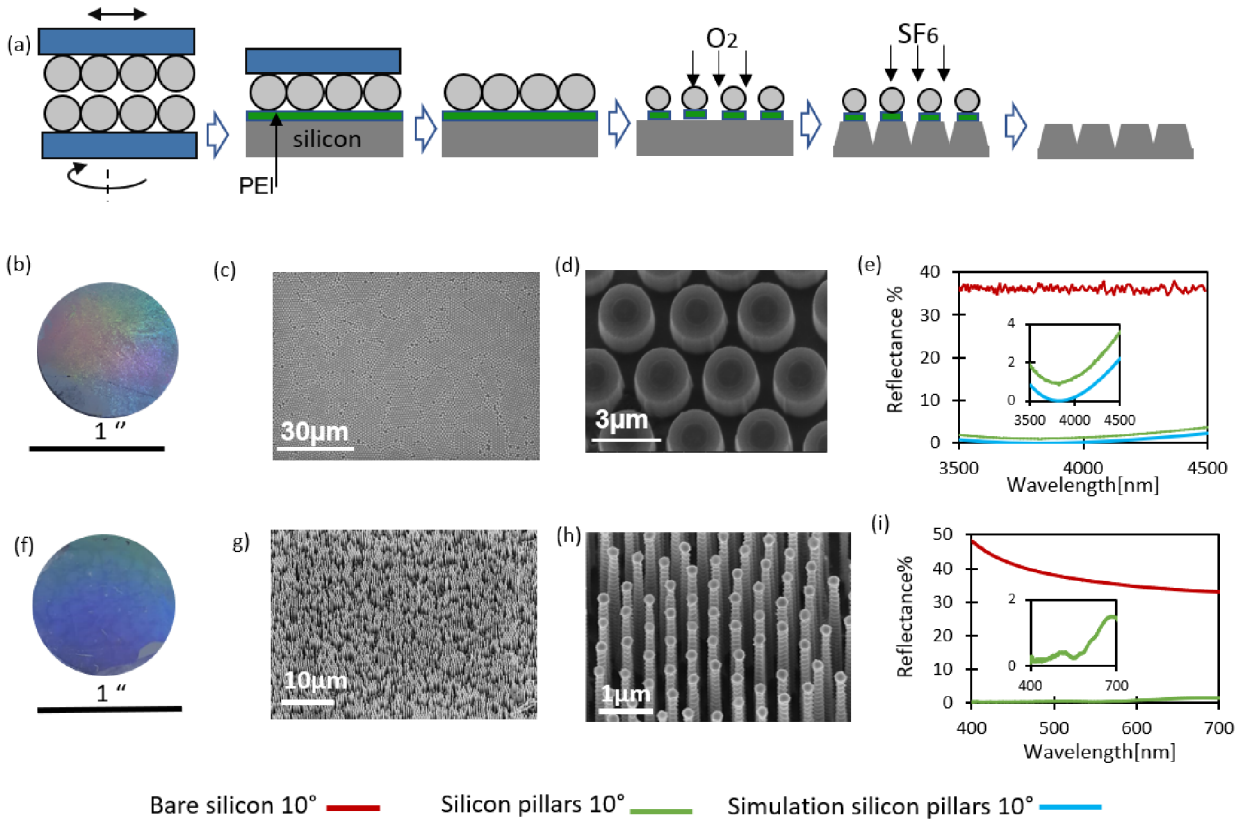


**Figure 2.** (a) Process flow of the fabrication of antireflective structures. (b)−(d) Moth-eye structures on silicon designed for mid-IR spectrum. (e) Optical characterization of moth-eye structures on silicon in mid-IR, compared to bare silicon. (f)−(h) Antireflective structures on silicon active in the visible spectrum. (i) Optical characterization of antireflective structures on silicon in the visible spectrum, compared to bare silicon.

surface rotates, and the upper surface moves in a linear direction in an oscillatory manner (Figures 1b and S1). Such movement produced the most effective and uniform evacuation of the excess particles from the interface between the two elastomers, resulting in almost defect-free particle monolayers on both surfaces (Figure S2). The obtained monolayer is uniform through the elastomer substrate, with no observable edge effect (Figure S3). The monolayer is formed quickly, usually within a few seconds, as can be monitored by microscope imaging of the rubbed surfaces at the intermediate stages (Figure S4). Furthermore, such a combined rotational-translational movement can be performed either manually or automatically. For the latter case, we used a commercial precision lens polisher (Strassbaugh 6Y) (Supplementary movie 1), as well as a home-built lapping tool. The critical process conditions, such as the pressure between the two surfaces, as well as the movement direction, periodicity, speed, and amplitude, can be precisely controlled, and this control ensures the high repeatability of the process and its tunability to the particle size. The used PDMS (Sylgard 184) was obtained by mixing the resin and the hardener in the standard ratio of 10:1, which produces the elastic modulus of a few MPa. To check whether the PDMS modulus has an effect on the quality of the obtained particle monolayer, an experiment was conducted using PDMS obtained at a 5:1 ratio, which produces a few times higher modulus.[34] However, this change in the PDMS modulus produced no observable effect on the particle monolayer (Figure S5), thus standard 10:1 ratio was used for all the experiments described below. Notably, to avoid possible contamination, the assembly process and all of the follow-up procedures were done in a clean hood with filtered air. Particularly, contaminations in the form of particles larger than the nanospheres used in the assembly, or the agglomeration of nanospheres, can cause scratches in the formed particle monolayer. Thus, the cleaning of the rubbed powder, as well as of the environment in which the process is done, is critical for obtaining a high-quality monolayer.

The rubbing approach has been so far limited to producing particle monolayers on the surface of elastomers such as PDMS. However, for practical applications, it is highly desired to produce such monolayers on the surface of other functional materials on which they can be used, for instance, as lithographic masks. To achieve this, we developed a process for the transfer of the particle monolayer from elastomer to any target substrate. In this process, the target substrate is first coated by a thin film of a molecular glue that electrostatically attracts the particles, whose zeta potential is around −30 mV (the exact values appear in Table S1). Then, the target substrate is controllably pressed against the elastomer surface covered with the monolayer. Then, the elastomer is pilled off, leaving the nanoparticles attached to the target substrate. We found that polyethylendiamine (PEI), which is dissolved in ethanol and applied onto the target surface by spin-coating as a thin layer with controllable thickness, acts as a highly efficient molecular glue and enables full transfer of the nanoparticles onto the target surface. The excess PEI can be later removed by soaking the target substrate with the nanoparticle in ethanol for a few hours at room temperature, making the particle monolayer on the target substrate ready for the further pattern transfer process. Using this approach, we successfully trans-


https://doi.org/10.1021/acsami.3c18554
ACS Appl. Mater. Interfaces 2024, 16, 17846−17856

ferred monolayers of nanoparticles of different sizes, from 200 nm to 2 $\mu$m, on both flat and curved surfaces (Figure 1b−e). In this work, we used two types of target surfaces, silicon and sapphire, as described below; however, the method is not limited to these materials and is applicable on any solid surface. The target surface was pretreated with short oxygen plasma to facilitate the wetting and adhesion of PEI. We kept the same process conditions for all the probed particle sizes (see details in Materials and Methods), while the only parameter that was varied with the particle size was the PEI thickness that was always ∼20% of the particle diameter. A cross-section SEM image of the transferred monolayer is provided in Figure S6 to demonstrate the formation of monolayer crystals.

We must notice that the transfer process produces almost defect-free pattern with polycrystalline structure (Figure S7). To demonstrate this, we imaged large areas of around half $mm^2$, and analyzed defects (Figure S1). To discriminate between the defects and the naturally occurring grain boundaries of the polycrystalline monolayer of particles, we defined the defects as any area uncovered by particles that is larger than an ellipse with the minor axis equal to or larger than the particle diameter (Figure S2). We found that the average defect density is around 0.65%. For comparison, previously reported approaches of colloidal assembly on the dry transfer of particles produced up to 5% defects,[35] making them unlikely to be applicable for the uses described hereafter, such as high-performance antireflective structures.

Finally, the obtained monolayers were analyzed by Voronoi tessellation broadly used to characterize the morphology of nanoparticle monolayers.[36] The tessellation is formed by identifying particle centroids as seeds and dividing the space into polygons, with each polygon encompassing points closer to one seed than others. This analysis offers the benefit of obtaining a clear visualization of the symmetry within the particle arrangement and the types of its defects, allowing us to assess the regularity indices and the areal disorder factors of the particle monolayers before and after the transfer. We analyzed both monolayers of particles right after rubbing on PDMS and after the transfer (Figures 1g,h and S8). The obtained polygonal arrays were characterized in terms of Voronoi Regularity Index (RI), which is defined as the ratio of the standard deviation of the areas to the average area of the polygon, which was found to be equal to 0.13 ±0.04 and 0.12 ± 0.04 for the as-rubbed and transferred particle monolayers, respectively. Also, the areal disorder factor was calculated for both cases. The areal disorder factor is defined as

$$\mathrm{AD} = 1 - \left(1 + \frac{\sigma}{\bar{A}}\right)^{-1} \quad (1)$$

where $\bar{A}$ and $\sigma$ are the average and standard deviation of the polygon area within the array, respectively, whereas AD = 0 represents perfect order of the particles. For the analyzed arrays of rubbed and transferred nanoparticles, AD was found to be, on average, 0.11± 0.03 and 0.13 ± 0.03. The similarity between the regularity indices and the areal disorder factors of the arrays before and after transfer indicates that the transfer does not cause any substantial change in the array morphology and largely maintains the polycrystalline order obtained by rubbing.

We demonstrated this new fabrication approach on several applications. One of them is a high-throughput fabrication of moth eye antireflective structures[37] (Figure 2a). Two examples here show moth-eye antireflective structures on silicon, which were designed for the mid-IR (3.7−4.3 $\mu$m) and visible spectra and were fabricated using polystyrene spheres with a diameter of 1 $\mu$m and 500 nm, respectively (Figure 2b−d and f−h). In both cases, the particle monolayer was first applied on PDMS by the above-described method, and then transferred from PDMS to silicon. The further pattern transfer included the trimming of the PS particles by oxygen plasma etching, followed by silicon plasma etching though the formed PS particle mask, and the removal of the particles by rinsing with chlorobenzene. It must be noted that moth-eye structures for the infrared region were designed in accordance with the effective medium approach,[38] by which the subwavelength periodicity produces an effective antireflective layer with a smooth index gradient. This approach is valid when the periodicity of structures is substantially smaller than the wavelength. This gradient can be verified by the cross-sectional SEM of etched structures (Figure S9). It must be noted, that the little defects observable in the SEM image are significantly smaller than the wavelength for which the antireflective structures are designed, therefore their effect on the antireflective performance due to the scattering is negligible.[39] Figure 2e shows the reflection spectrum for the angle of incidence 10°. The reflectance reaches its minimum around 3800 nm and gradually increases for higher and lower wavelengths, as predicted by the simulated spectra based on the effective medium theory. The difference of ∼1% in the reflection intensity between the simulated and experimental spectra can be attributed to the slight deviation in the obtained profile of etched structures from that of the design. The reflection spectra taken at the higher angles of 30° and 40° (Figure S10) show higher reflection, in accordance with higher reflection, in accordance to the effective medium theory shown in the simulations. On the contrary, the structures for the visible spectrum are based on the scattering,[26] in which the antireflective effect improves the angle of incidence (Figures 2i, S11). Overall, in both cases, the fabricated structures produce antireflective effects comparable to that of the state-of-the-art moth-eye structures fabricated by colloidal lithography and other methods.[40,41]

It must be noted, that the antireflective effect achieved by our method—for both IR and visible ranges—is quantitatively comparable or better than that achieved by similar antireflective structures fabricated by methods, such as electron beam lithography and nanosphere lithography based on Langmuir−Blodgett deposition.[29,42,43] However, both electron beam lithography and Langmuir−Blodgett deposition are extremely low-throughput methods, which are incompatible with practical optical applications. For instance, patterning on one square inch surface by Langmuir−Blodgett takes a few hours, while electron beam patterning usually takes even much longer, depending on the pattern resolution and density. Furthermore, electron beam lithography requires expensive equipment and precise control over the process conditions, which further limits its usage beyond making low-cost prototypes. Additional methods are based on novel lithographic approaches, such as Displacement Talbot Lithography (DTL),[44] which, however, requires sophisticated tooling and expensive mask with submicron resolution. On the contrary, our methodology requires no sophisticated equipment or mask and produces large area patterns within a few minutes, which makes it highly suitable for optical applications. Furthermore, it can be easily scaled up for high-throughput production,


https://doi.org/10.1021/acsami.3c18554
ACS Appl. Mater. Interfaces 2024, 16, 17846−17856

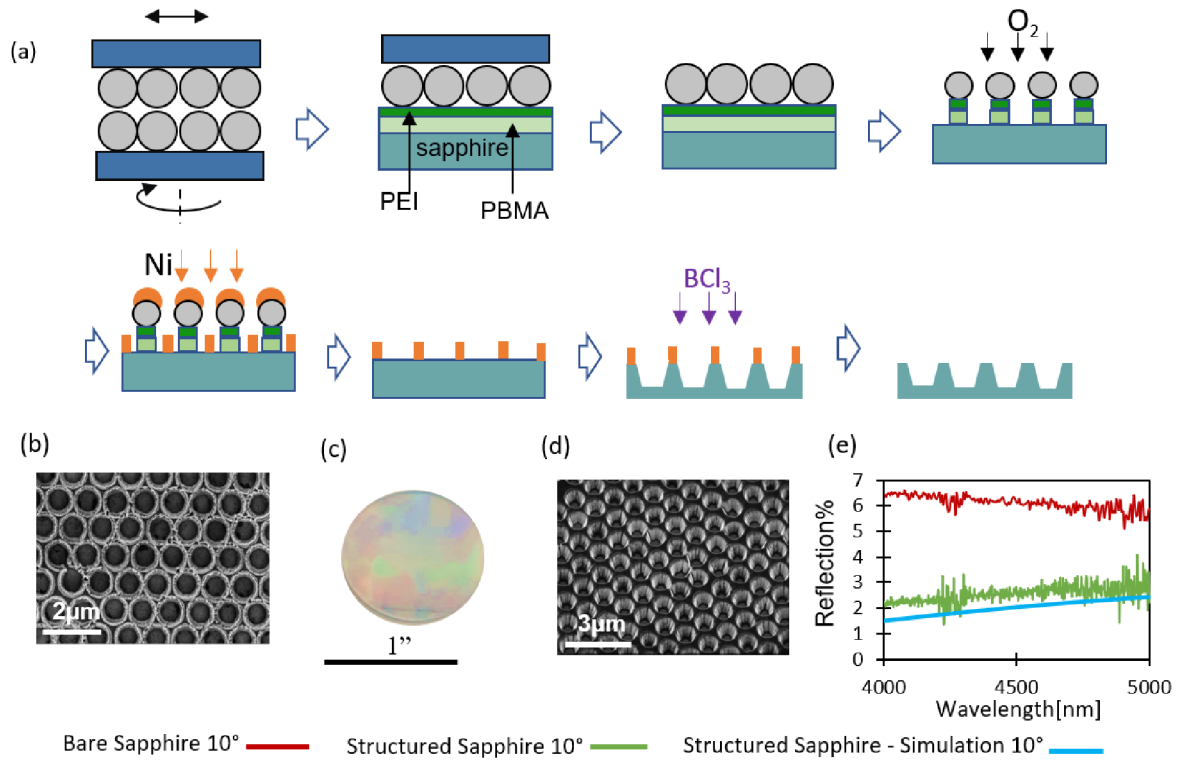


**Figure 3.** (a) Schematic process flow of the fabrication of antireflective hole arrays on sapphire. (b) SEM of Ni mask after the liftoff, (c) sapphire substrate with patterned antireflective structures, (d) SEM antireflective structures, and (e) reflection spectrum of patterned sapphire at 10° angle of incidence vs bare sapphire.

without compromising on the functional performance of the obtained nano/microstructures, as we demonstrated here. Also, antireflective structures can be produced at a low cost by maskless etching.[45] However, this method cannot control the structure geometry, which precludes the precise optical design of these structures and its optimization for a specific range of wavelengths. Furthermore, structures produced by maskless etching are fragile, which substantially restricts their applications to scenarios that preclude physical contact. On the contrary, the method shown here allows precise implementation of the optical design and produces mechanically robust structures, as demonstrated hereafter.

The most common design of moth-eye antireflective structures is based on conically shaped bumps, which are bioinspired from nanometric bumps on the cornea of a nocturnal moth.[46] Alternatively, antireflective structures with similar optical functionality can also be realized as an array of holes with subwavelength diameter as soon as the air-material volume-ratio, which determines the effective refractive index in the formed antireflective layer, matches the optical design. The arrays of holes are attractive for optics due to their mechanical durability; however, their fabrication is more complicated than that of bumps. Here, we demonstrate that our approach for particle lithography can be successfully used to produce hole-shaped antireflective structures in sapphire. Sapphire is a broadly used optical material, especially in high-end optics and also in consumables such as windows of luxury watches and cameras in mobile phones because it combines excellent optical transmittance with mechanical and environmental stabilities. At the same time, reflection from sapphire must be prevented for most of its optical applications. Standard vacuum-deposited antireflective thin films on sapphire suffer from low mechanical stability and thermal expansion coefficient significantly different from sapphire's. The latter produces thermal stresses that, in turn, lead to cracks and delamination. Alternatively, moth-eye structures offer an attractive antireflective solution for sapphire, but their fabrication is extremely challenging due to the difficulty of Sapphire etching by plasma. So far, scalable plasma-etched moth-eye structures on sapphire were demonstrated only for the visible spectrum, where the etching depth typically does not exceed 200 nm.[47] On the other hand, sapphire is also broadly used in mid-infrared applications. Yet, moth-eye structures for such wavelength range, whose vertical dimension should be almost one micron or more, depending on the desired wavelength, have been demonstrated only by direct laser writing,[48,49] which is highly unscalable and impractical.

Here, we demonstrate that our novel colloidal lithography approach can provide a solution for the scalable fabrication of moth-eye structures on sapphire for the mid-infrared spectrum (Figure 3a). As previously stated, the colloidal monolayer was transferred from the elastomer to sapphire, which was precoated with 200 nm film of polybenzyl methacrylate (PBMA) and 300 nm of PEI. The sphere transfer was followed by the removal of the excess PEI by soaking in ethanol for a few hours and etching with oxygen plasma, which had three purposes: (i) reducing the size of PS spheres, (ii) removal of the excess PEI, and (iii) etching of PBMA in the open areas. This etching also produces an undercut in PBMA (Figure S12). Then, 330 nm of nickel—a commonly used masking material for sapphire plasma etching—was deposited by e-gun evaporation, and a mesh-like nickel mask was obtained after liftoff. The thickness of the nickel mask was chosen based on the known Ni−sapphire selectivity at 1:3 ratio in $BCl_3$ plasma, which was used to etch sapphire, and it to ensure that the mask did not disappear during the etching process. It must be noted


https://doi.org/10.1021/acsami.3c18554
ACS Appl. Mater. Interfaces 2024, 16, 17846−17856

that the PBMA sacrificial layer was used here to elevate the particles above the sapphire surface. Furthermore, the etching rate of PBMA in oxygen plasma is about three times higher than that of polystyrene. Thus, while the polystyrene nanoparticles are trimmed to the desired diameter, an undercut in PBMA is formed. This undercut ensures successful liftoff after the deposition of such a thick nickel film (Figure 3b), eliminating the need to control the exact etching profile of PBMA. Notably, due to relatively low plasma etching rate of sapphire, its patterning requires extremely thick mask with extreme aspect ratio of masking features, which substantially complicates the fabrication process.[50] Our innovative usage of a sacrificial layer with an undercut allowed us to circumvent this limitation and obtain a robust low-aspect ratio metal mask. Finally, sapphire was plasma-etched to obtain 800 nm deep holes (Figure S13), and the rest of the nickel mask was removed by hot Piranha solution. Figure 3c,d shows the hole-based arrays of sapphire's moth-eye structures. Figure 3e shows the reflection spectrum of the patterned sapphire vs that of bare sapphire and the theoretical spectrum of sapphire's moth-eye structures obtained by simulations based on the effective medium theory. Reflectance measurements at higher angles are shown in Figure S14. It can be seen that the fabricated structures reduced the reflection in the desired spectral range from ∼7% down to ∼2%. We believe this reflection can be reduced by further optimizing the geometry of antireflective structures.

We want to emphasize that while state-of-the-art moth-eye structures fabricated by methods, such as electron beam lithography, interference lithography, or Langmuir−Blodgett assembly are unlikely to be suitable for practical optical applications due to low throughput and high cost, today's more scalable and cost-effective alternative to these structures can be provided by randomly shaped antireflective structures. These randomized structures can be produced by either maskless plasma etching[51] or etching through a mask formed by dewetting of metallic films.[52] Today, randomized antireflective structures are commercially available. However, their main drawback is that they are highly fragile due to their uncontrolled shape and high-aspect ratio. This fragility makes the optical surface of these structures completely intolerable to any mechanical contact. For instance, such surfaces cannot be cleaned by any method commonly used in optics that involves wiping, substantially limiting the applications of these structures. Here, we demonstrated that the moth-eye structures produced by our method possess extreme mechanical stability and can also withstand mechanically aggressive clearing. To test the mechanical stability, we performed a commonly used pencil test. A line was drawn on the patterned surface with a pencil of HB hardness. Then, the same area was wiped with cleaning paper soaked in isopropyl alcohol, dried, and wiped again with a rubber eraser. Naturally, wiping paper and erasing did not remove the graphite line drawn by the pencil from the surface. Finally, the graphite was entirely removed by immersing the surface in hot piranha solution for 10 min, followed by water rinsing and drying. Microscopic observation of the drawing area showed that the surface pattern structure shape was unaffected by the pencil drawing and the subsequent attempts to clean it (Figure S15). Overall, these findings emphasize that the new nanolithography method provides a technological route to highly cost-effective antireflective nanostructures with mechanical durability that is unachievable by commercially available antireflective structures.

It should be noted that the described method of rubbing followed by the particle transfer produces a polycrystalline structure, which is well-suited for optical applications like antireflective structures. Besides these optical nanostructures, high-throughput production of periodic nanopatterns with polycrystalline structures can be used in endless applications, especially in biology and biomedicine. These emerging applications include, but are not limited to, the fabrication of high-resolution biosensors for the detection of various biomarkers and analytes,[53] the fabrication of precisely patterned surfaces that can influence cell behavior and guide tissue growth,[54,55] as well as promote cell adhesion[56,57] and differentiation,[58] thereby facilitating the development of functional tissues. Overall, the applications of particle lithography in biomedicine hold immense potential for advancing diagnostics, tissue engineering, and therapeutic interventions.

In this work, we chose one specific biomedical application to demonstrate the versatility of our lithography method. In recent years, immunotherapeutic applications of T cells have gained significant attention in cancer treatment. One notable approach is adoptive cell transfer (ACT), in which T cells are isolated from a patient, genetically engineered, or modified to enhance their targeting capabilities, and then reinfused into the patient's body.[59,60] These modified T cells can effectively target and destroy cancer cells, leading to remarkable responses in patients with certain hematological malignancies. The ability to genetically modify T cells and enhance their therapeutic potential greatly relies on their ex vivo activation and proliferation. This activation is commonly done with magnetic polymer microbeads covered with antibodies against activating and costimulatory receptors. However, such beads have been initially developed for selective cell separation, and neither their shape nor their mechanical properties have ever been optimized for T cell activation. In the past decade, there have been intensive research aimed at developing new material-based approaches for the effective ex vivo activation of T cells.[61−65] One such approach was recently demonstrated by us wherein a surface was structured with a periodic array of elastic micropillars, which produced much more effective activation and proliferation of T cells than those produced by standardly used magnetic beads.[66] However, the fabrication of such arrays on elastomer casting from a mold produced by electron beam lithography is a low-throughput method unsuitable for producing a cell activating area sufficient for a therapeutic amount of T cells. The limitation of electron beam lithography for this application is stressed by the fact that a typical single dose of genetically modified T cells is $10^7-10^9$ cells.[67] Given that the surface density of T cells on the activating surface is ∼1.8 million cells/cm$^2$, a therapeutic amount of $10^8$ T cells would require an activation surface with an area of around 55 cm$^2$. Even if a high-power electron beam lithography tool with a typical beam current of 100 nA is used, production of such an area would take about 12 h (detailed calculation appears in the Supporting Information). This is an impractical fabrication time, which is a crucial bottleneck in implementing this nanotechnological approach for activating T cells. Other nanoscale structures for the activation lymphocytes can be produced from the bottom-up, in the form of vertically grown inorganic nanowires.[68−71] However, the fabrication of such nanostructures is slow—it usually takes a few hours to grow vertical nanowire forest on a small surface by chemical vapor deposition. Furthermore, due to their small diameter, nano-


https://doi.org/10.1021/acsami.3c18554
ACS Appl. Mater. Interfaces 2024, 16, 17846−17856

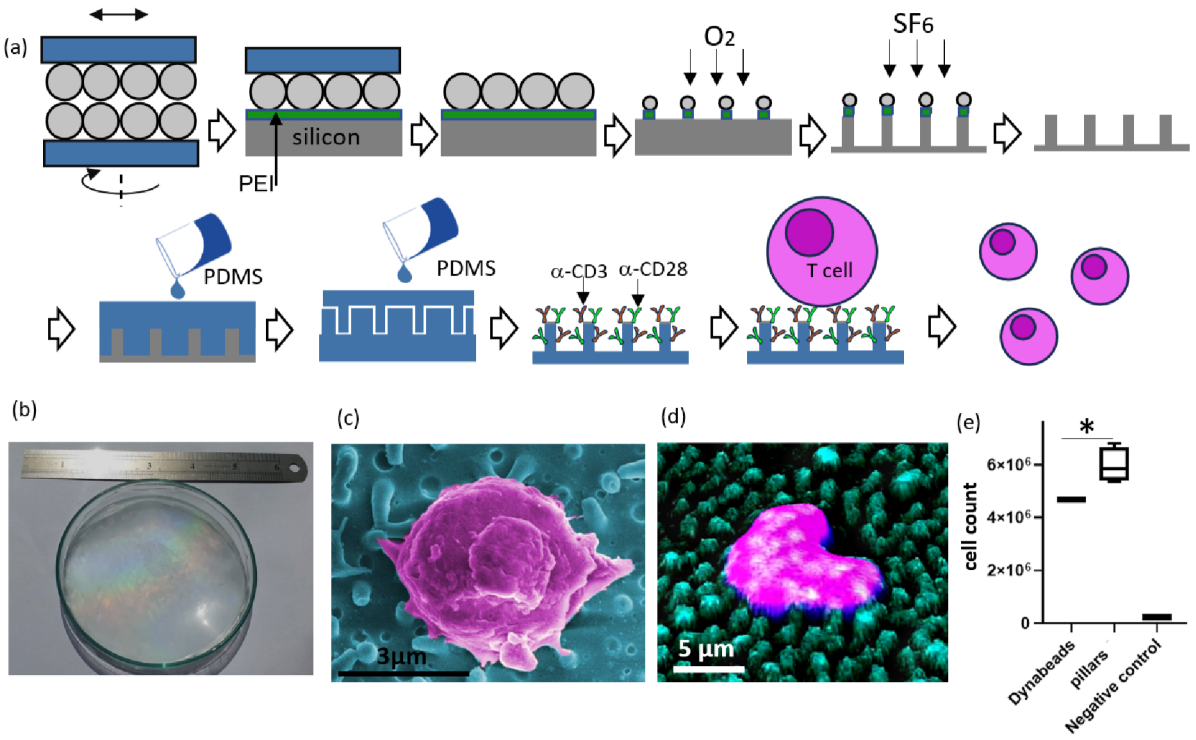


**Figure 4.** (a) Fabrication process flow of the antibody-functionalized elastic pillars for the activation of T cells. (b) Scalable platform for T cell activation fabrication by dry rubbing implemented by a Petri dish with a diameter of 10 mm. (b and (c) SEM and confocal images of T cells stimulated on the elastic pillars. (e). Proliferation of T cells after 7 days: the amount of proliferated T cells (per 2 mL of medium) activated on the pillars is compared to that of T cells activated using antibody-functionalized magnetic beads (Dynabeads) and that of T cells activated on clean Petri dish (negative control). The data were obtained in triplicates, and analysis was performed with Tukey's multiple-comparison tests using the GraphPad Prism software. *$p < 0.05$.

wires deeply invaginate into the cell membrane, which prevents cell detachment from nanowires upon activation. The latter limitation makes the nanowire impractical for cell proliferation and immunotherapeutic usage upon activation.

Here, we showed that our new nanopatterning method can address the above-mentioned limitation of e-beam lithography for fast and scalable production of elastomer-based brush arrays for the activation of T cells. To that end, we assembled 2 $\mu$m polystyrene microspheres on PDMS, transferred the obtained microsphere monolayer to silicon substrate, etched silicon through the formed microsphere mask to obtain an array of silicon pillars, with the height of ~2.5 $\mu$m, bottom diameter of 800 nm, and top diameter of 300 nm. We then transferred this 3D pattern to PDMS by double replication, as described in detail in the experimental section (Figure 4a). Using this approach, we could produce activating surfaces for T cells as large as fitting the bottom of 100 mm cell culture dish, which can accommodate ~$1.4 \times 10^8$ cells (Figure 4b).

For the activation of T cells, we coated the surface of the PDMS pillars with anti-CD3 and anti-CD-28, which trigger the activating and costimulatory receptors of T cells, respectively, using a previously reported protocol.[66] We isolated primary T cells for the peripheral blood of a healthy donor and stimulated them for 24 h on the activating surface. Figure 4c,d shows the electron micrograph and z-stack confocal micrograph, respectively, of a typical T cell stimulated on the pillar array. Notably, some pillars appear to be bent in SEM, which is an artifact of the drying effect,[72] and this effect is not seen in the confocal microscopy image, in which the cell and the structures have been fixed prior to imaging. It is clearly seen that the T cell forms contact with the top of the pillars and applies centripetal forces that are clearly detectable due to the relatively high elastic response of the pillars to these forces. We previously showed that the response of vertical elastic microstructures to these forces is critical for the activation of lymphocyte cells.[68−71] Here, we examined the effect of the elastic microstructures produced by colloidal lithography on the proliferation of T cells. The T cells were activated for 24 h on the pillars and transferred to a culture dish for proliferation. The proliferation lasted 7 days, during which interleukin was added to the culture medium on a daily basis. Figure 4e shows the proliferation of T cells activated on the pillars in comparison to control groups—T cell activation on bare Petri dishes (negative control) and T cells activated using commercially activating magnetic beads (Dynabeads TM). Overall, elastic pillars produced a substantially higher proliferation rate of T cells as compared to beads, which stemmed from the superior mechano-stimulating ability. This ability, in turn, was caused by two independent factors (i) the elastic compliance of the activating surface to the forces applied by cells,[73] and the microtopography that induces the formation of microvilli in T cells, which regulate signaling and gene expression in T cells.[74] The results shown here demonstrated that harnessing mechanotopographical stimulation in immunotherapy can be implemented in a scalable manner, using the high-throughput activation method described in this paper. Furthermore, an important insight into the T cell mechano-stimulating topography, beyond its fabrication, refers to its structure. Whereas elastic pillars have been previously used for interactions with living cells for mechanobiological studies in general,[75] and T cell studies in particular,[76] all of them were fabricated by top-down


https://doi.org/10.1021/acsami.3c18554
ACS Appl. Mater. Interfaces 2024, 16, 17846−17856

lithographic approaches with strict period structure and long-range order. Here, we demonstrate that the pillars can be configured into a polycrystalline array with a short-range order, without compromising on their functionality, which is the activation and proliferation of T cells in this case.

## CONCLUSIONS

In summary, we have demonstrated a versatile and robust nanofabrication approach. Its great advantage, as compared to the common bottom-up fabrication based on the nanostructure assembly from liquid to solid phases, is its simplicity, high throughput, and scalability. Whereas previously demonstrated dry assembly of colloids was restricted to the formation of monolayer of elastomer (PDMS) substrates, with limited applications, our work unleashes this attractive fabrication approach from elastomer substrate constraints and enables its implementation to substrates of any solid material. Besides its high speed, the presented assembly process is superior to the state-of-the-art assembly process due to its high robustness. For instance, colloidal lithography based on Langmuir–Blodgett self-assembly is highly sensitive to particle size and composition of the solvent, and it requires tight environmental control and accurate in situ monitoring of the process parameters, such as the surface tension and speed of the sample extraction.[77] On the contrary, the colloidal lithography process described in this paper has a very wide process window and very low sensitivity to its process parameters, such as rubbing motion as well as the pressure and time of the transfer process. The automatic rubbing process can be done in a highly scalable manner using existing equipment that is originally designed for polishing or rubbing, as we demonstrated in this paper. This equipment allows easy and accurate control over the process conditions, such as pressure and rotation speed. Thus, the existing infrastructure can be used to increase the scalability of this fabrication approach. The two applications demonstrated here—one in the field of optics and another in the field of the manipulation of immune cells—illustrate the high versatility of this approach. Overall, this novel lithography process opens a pathway to precise, scalable, and high-throughput fabrication of endless micro/nanoscale devices and systems.

## MATERIALS AND METHODS

**Rubbing of Particle Monolayer on PDMS.** The PDMS (Sylgard 184) surface was prepared by mixing PDMS and its hardener in 1:10 ratio (unless otherwise specified), with casting on polished silicon wafer and curing at 60 °C for 1 h, to obtain an elastic modulus of around 1.5 MPa. The cure PDMS was cut to desired sizes, then a small amount (~0.3 mg per sq. inch) of the nanoparticle powder was placed between two PDMS surfaces and rubbed, with the translational movement of the upper surface and rotational movement of the lower surface. The rubbing itself was done either manually or using a lapping tool, with the controlled rotation of 30 rpm and translational frequency of 0.5 Hz.

**Transfer of Particles from PDMS.** The target surface was first exposed to the $O_2$ plasma for 40 s (Harrick plasma) and then spin coated with a thin film of PEI dissolved in ethanol. Different degrees of dilutions were used to achieve PEI thickness of about 20% of the diameter of the used spheres. The nanoparticle monolayers were transferred to the target surface by bringing it in contact with PDMS, and applying pressure of 2 bar for 30 s, using a homemade nanoimprint machine. Finally, the elastomeric surface was peeled off and the particle monolayers were fully transferred to the solid surface.

**Pillar-Like Antireflective Coating on Silicon.** For the antireflective structures on silicon in the visible spectrum, the nanosphere size was first reduced from 500 to 350 nm by dry etching in $O_2$ plasma (Oxford Plasmapro 100 Cobra, 70 sccm $O_2$, RF = 116 W, $p$ = 19 mTorr, 1:46 min). Then, the nanosphere pattern was transferred to silicon by dry etching using a Bosch process (Oxford Plasmapro 100 Estrella). Finally, the remaining microspheres were removed by sonication in chlorobenzene.

For the antireflective structures on silicon in the mid infrared spectrum, the nanosphere size was first reduced from 1000 to 860 nm by dry etching in $O_2$ plasma (Oxford Plasmapro 100 Cobra, 70 sccm $O_2$, RF = 100 W, $p$ = 15 mTorr, 3 min). Then, the nanosphere pattern was transferred to silicon by dry etching using (Oxford Plasmapro 100 Estrella, RF = 20 W, ICP = 800, $p$ = 10 mTorr, $C_4F_8$ = 50 sccm, $SF_6$ = 25 sccm, $t$ = 3 min). Finally, the remaining microspheres were removed by sonication in chlorobenzene.

**Pillar-Like Antireflective Coating on Sapphire.** Sapphire was first coated by PBMA using spin coating, and then covered by an array of 1 $\mu$m polystyrene particles. Then, dry etching by $O_2$ plasma (Oxford Plasmapro 100 Cobra, 70 sccm $O_2$, RF = 100 W, $p$ = 15 mTorr, $t$ = 3:45 min) was used to reduce the particle diameter to 820 nm and create an undercut in PBMA. 330 nm nickel film was deposited by e-gun evaporation, following liftoff to obtain a Ni mask. Sapphire was etched through the mask (Oxford Plasmapro 100 Cobra, RF = 200 W, ICP = 1750, $p$ = 2 mTorr, $BCl_3$ = 25 sccm, $t$ = 6 min), and finally, Ni was removed by piranha solution.

**Platform for T Cell Activation.** Silicon master mold was produced using 2 $\mu$m diameter polystyrene microspheres. The microsphere diameter was reduced to 800 nm by dry etching in $O_2$ plasma (Oxford Plasmapro 100 Cobra, 70 sccm $O_2$, RF = 100 W, $p$ = 20 mTorr, 12 min). Then, the microsphere pattern was transferred directly to the silicon by etching the silicon through the sphere mask (Oxford Plasmapro 100 Estrella mix gas, ICP = 800 W, RF = 20 W, $SF_6$ = 25 sccm, $C_4F_8$ = 25 sccm, $p$ = 10 mTorr, $t$ = 2 min). The remaining microspheres were removed by sonication in chlorobenzene. The following steps included coating the mold with antiadhesive agent, double replication with PDMS, and PDMS coating with activating and costimulatory antibodies, as described in our previous work.[66] Peripheral blood mononuclear cells (PBMCs) were isolated from blood using the FICOL gradient. First, blood was diluted with PBS augmented with 2% fetal bovine serum (FBS), at a 1:1 ratio, then loaded on FICOL gradient, and centrifuged at 16 °C at 1200$g$ (with no breaks or acceleration). The PBMCs were collected as the middle disc and a small portion of the underlying phase but taking care not to withdraw the pellet, washed three times with at least 1:2 with PBS 2% FBS at room temperature, and sedimented at 500 g. The cells were finally suspended in the final medium in the ratio of 2 mL per 7 mL of collected blood, counted, and diluted with the medium to final concentration of $1 \times 10^6$ cells per mL. The cells were then seeded onto PDMS surfaces in the growth medium containing <2% serum and 50 units of IL-2 and left inside incubator to adhere for 24 h. Then, the cells were transferred to 48-well plate. After 7 days, the cells were counted using trypan blue (1:1 diluted) to check the proliferation on DeNovix CellDrop.

## ASSOCIATED CONTENT

### Supporting Information

The Supporting Information is available free of charge at https://pubs.acs.org/doi/10.1021/acsami.3c18554.

Calculation of time for electron beam lithography, values of zeta potential of the used nanoparticles, comparison of different rubbing movements, defect analysis of the rubbed monolayer, analysis of the edge effect, development of the particle monolayer with time, analysis of the effect of PDMS elasticity on the monolayer quality, cross section imaging of the transferred monolayer, analysis of polycrystalline structure of the particle monolayer, morphology characterization by Voronoi Tessellation, profile of the etched structured in silicon, reflection spectra of the fabricated antireflective structures, AFM



https://doi.org/10.1021/acsami.3c18554
ACS Appl. Mater. Interfaces 2024, 16, 17846−17856

and SEM images of the antireflective structures on sapphire, and the results of the pencil-based durability test (PDF)

(MP4)

## AUTHOR INFORMATION


### Corresponding Author

**Mark Schvartzman** − *Department of Materials Engineering, Ben-Gurion University of the Negev, Beer-Sheva 84105, Israel; Ilse Katz Institute for Nanoscale Science and Technology, Ben-Gurion University of the Negev, Beer-Sheva 84105, Israel;* orcid.org/0000-0002-5912-525X; Email: marksc@bgu.ac.il

### Authors

**Sivan Tzadka** − *Department of Materials Engineering, Ben-Gurion University of the Negev, Beer-Sheva 84105, Israel; Ilse Katz Institute for Nanoscale Science and Technology, Ben-Gurion University of the Negev, Beer-Sheva 84105, Israel*

**Carlos Ureña Martin** − *Department of Materials Engineering, Ben-Gurion University of the Negev, Beer-Sheva 84105, Israel; Ilse Katz Institute for Nanoscale Science and Technology, Ben-Gurion University of the Negev, Beer-Sheva 84105, Israel*

**Esti Toledo** − *Department of Materials Engineering, Ben-Gurion University of the Negev, Beer-Sheva 84105, Israel; Ilse Katz Institute for Nanoscale Science and Technology, Ben-Gurion University of the Negev, Beer-Sheva 84105, Israel;* orcid.org/0000-0003-3103-816X

**Abed Al Kader Yassin** − *The Shraga Segal Department of Microbiology, Immunology, and Genetics Faculty of Health Sciences, Ben-Gurion University of the Negev, Beer-Sheva 84105, Israel*

**Ashish Pandey** − *Department of Materials Engineering, Ben-Gurion University of the Negev, Beer-Sheva 84105, Israel; Ilse Katz Institute for Nanoscale Science and Technology, Ben-Gurion University of the Negev, Beer-Sheva 84105, Israel*

**Guillaume Le Saux** − *Department of Materials Engineering, Ben-Gurion University of the Negev, Beer-Sheva 84105, Israel; Ilse Katz Institute for Nanoscale Science and Technology, Ben-Gurion University of the Negev, Beer-Sheva 84105, Israel;* orcid.org/0000-0003-4902-1980

**Angel Porgador** − *The Shraga Segal Department of Microbiology, Immunology, and Genetics Faculty of Health Sciences, Ben-Gurion University of the Negev, Beer-Sheva 84105, Israel*

Complete contact information is available at: https://pubs.acs.org/10.1021/acsami.3c18554



### Funding

This work was supported by the Israel Innovation Authority.


### Notes

The authors declare no competing financial interest.

## REFERENCES


(1) Vanderhoff, J. W. Mechanism of Emulsion Polymerization. *J. Polym. Sci. Polym. Symp.* **1985**, *72* (1), 161−198.

(2) Lovell, P. A.; Schork, F. J. Fundamentals of Emulsion Polymerization. *Biomacromolecules* **2020**, *21* (11), 4396−4441.

(3) Goodall, A. R.; Wilkinson, M. C.; Hearn, J. Mechanism of Emulsion Polymerization of Styrene in Soap-free Systems. *J. Polym. Sci.* **1977**, *15*, 2193−2218.

(4) Winzer, M.; Kleiber, M.; Dix, N.; Wiesendanger, R. Fabrication of Nano-Dot- and Nano-Ring-Arrays by Nanosphere Lithography. *Appl. Phys. A: Mater. Sci. Process.* **1996**, *63* (6), 617−619.

(5) Frey, W.; Woods, C. K.; Chilkoti, A. Ultraflat Nanosphere Lithography: A New Method to Fabricate Flat Nanostructures. *Adv. Mater.* **2000**, *12* (20), 1515−1519.

(6) Wang, Y.; Zhang, M.; Lai, Y.; Chi, L. Advanced Colloidal Lithography: From Patterning to Applications. *Nano Today* **2018**, *22*, 36−61.

(7) Ai, B.; Möhwald, H.; Wang, D.; Zhang, G. Advanced Colloidal Lithography Beyond Surface Patterning. *Adv. Mater. Interfaces* **2017**, *4* (1), 1600271.

(8) Junesch, J.; Sannomiya, T.; Dahlin, A. B. Optical Properties of Nanohole Arrays in Metal−Dielectric Double Films Prepared by Mask-on-Metal Colloidal Lithography. *ACS Nano* **2012**, *6* (11), 10405−10415.

(9) Hanarp, P.; Käll, M.; Sutherland, D. S. Optical Properties of Short Range Ordered Arrays of Nanometer Gold Disks Prepared by Colloidal Lithography. *J. Phys. Chem. B* **2003**, *107* (24), 5768−5772.

(10) Von Freymann, G.; Kitaev, V.; Lotschz, B. V.; Ozin, G. A. Bottom-up Assembly of Photonic Crystals. *Chem. Soc. Rev.* **2013**, *42*, 2528−2554.

(11) Jensen, T. R.; Malinsky, M. D.; Haynes, C. L.; Van Duyne, R. P. Nanosphere Lithography: Tunable Localized Surface Plasmon Resonance Spectra of Silver Nanoparticles. *J. Phys. Chem. B* **2000**, *104* (45), 10549−10556.

(12) Zhu, X.; Wang, W.; Yan, W.; Larsen, M. B.; Bøggild, P.; Pedersen, T. G.; Xiao, S.; Zi, J.; Mortensen, N. A. Plasmon−Phonon Coupling in Large-Area Graphene Dot and Antidot Arrays Fabricated by Nanosphere Lithography. *Nano Lett.* **2014**, *14* (5), 2907−2913.

(13) Cai, Y.; Ocko, B. M. Large-Scale Fabrication of Protein Nanoarrays Based on Nanosphere Lithography. *Langmuir* **2005**, *21* (20), 9274−9279.

(14) Madaria, A. R.; Yao, M.; Chi, C.; Huang, N.; Lin, C.; Li, R.; Povinelli, M. L.; Dapkus, P. D.; Zhou, C. Toward Optimized Light Utilization in Nanowire Arrays Using Scalable Nanosphere Lithography and Selected Area Growth. *Nano Lett.* **2012**, *12* (6), 2839−2845.

(15) Tang, J.; Wang, H.-T.; Lee, D. H.; Fardy, M.; Huo, Z.; Russell, T. P.; Yang, P. Holey Silicon as an Efficient Thermoelectric Material. *Nano Lett.* **2010**, *10* (10), 4279−4283.

(16) Vogel, N.; Weiss, C. K.; Landfester, K. From Soft to Hard: The Generation of Functional and Complex Colloidal Monolayers for Nanolithography. *Soft Matter* **2012**, *8* (15), 4044−4061.

(17) Lotito, V.; Zambelli, T. Approaches to Self-Assembly of Colloidal Monolayers: A Guide for Nanotechnologists. *Adv. Colloid Interface Sci.* **2017**, *246*, 217−274.

(18) Toolan, D. T. W.; Fujii, S.; J. Ebbens, S.; Nakamura, Y.; R. Howse, J. On the Mechanisms of Colloidal Self-Assembly during Spin-Coating. *Soft Matter* **2014**, *10* (44), 8804−8812.

(19) Ghosh, M.; Fan, F.; Stebe, K. J. Spontaneous Pattern Formation by Dip Coating of Colloidal Suspensions on Homogeneous Surfaces. *Langmuir* **2007**, *23* (4), 2180−2183.

(20) Han, W.; Lin, Z. Learning from "Coffee Rings": Ordered Structures Enabled by Controlled Evaporative Self-Assembly. *Angew. Chem., Int. Ed.* **2012**, *51* (7), 1534−1546.

(21) Tao, A. R.; Huang, J.; Yang, P. Langmuir−Blodgettry of Nanocrystals and Nanowires. *Acc. Chem. Res.* **2008**, *41* (12), 1662−1673.

(22) Joshi, K.; Muangnapoh, T.; Stever, M. D.; Gilchrist, J. F. Effect of Ionic Strength and Surface Charge on Convective Deposition. *Langmuir* **2015**, *31* (45), 12348−12353.

(23) Maenosono, S.; Dushkin, C. D.; Yamaguchi, Y.; Nagayama, K.; Tsuji, Y. Effect of Growth Conditions on the Structure of Two-Dimensional Latex Crystals: Modeling. *Colloid Polym. Sci.* **1999**, *277* (12), 1152−1161.

(24) Born, P.; Blum, S.; Munoz, A.; Kraus, T. Role of the Meniscus Shape in Large-Area Convective Particle Assembly. *Langmuir* **2011**, *27* (14), 8621−8633.

(25) Lazarov, G. S.; Denkov, N. D.; Velev, O. D.; Kralchevsky, P. A.; Nagayama, K. Formation of Two-Dimensional Structures from Colloidal Particles on Fluorinated Oil Substrate. *J. Chem. Soc., Faraday Trans.* **1994**, *90* (14), 2077−2083.
(26) Cai, J.; Qi, L. Recent Advances in Antireflective Surfaces Based on Nanostructure Arrays. *Mater. Horiz.* **2015**, *2* (1), 37−53.
(27) Chan, L. W.; Morse, D. E.; Gordon, M. J. Moth Eye-Inspired Anti-Reflective Surfaces for Improved IR Optical Systems & Visible LEDs Fabricated with Colloidal Lithography and Etching. *Bioinspiration Biomimetics* **2018**, *13* (4), 041001.
(28) Ji, S.; Song, K.; Nguyen, T. B.; Kim, N.; Lim, H. Optimal Moth Eye Nanostructure Array on Transparent Glass towards Broadband Antireflection. *ACS Appl. Mater. Interfaces* **2013**, *5* (21), 10731−10737.
(29) Gonzalez, F. L.; Morse, D. E.; Gordon, M. J. Importance of Diffuse Scattering Phenomena in Moth-Eye Arrays for Broadband Infrared Applications. *Opt. Lett.* **2014**, *39* (1), 13−16.
(30) Le Cunff, L. O.; Kadiri, H.; Lérondel, G. Microscopic Defects as the Limiting Factor in the Direct Transmission of Nanocoatings Obtained through Self-assembly. *Nano Select* **2021**, *2* (1), 140−145.
(31) Dimitrov, A. S.; Miwa, T.; Nagayama, K. Comparison between the Optical Properties of Amorphous and Crystalline Monolayers of Silica Particles. *Langmuir* **1999**, *15* (16), 5257−5264.
(32) Iler, R. K. The Adhesion of Submicron Silica Particles on Glass. *J. Colloid Interface Sci.* **1972**, *38* (2), 496−500.
(33) Park, C.; Lee, T.; Xia, Y.; Tae, J. S.; Myoung, J.; Jeong, U. Large-Area Assembly of a Single-Crystal Monolayer of Spherical Particles by Unidirectional Rubbing. *Adv. Mater.* **2014**, *26* (27), 4633−4638.
(34) Moustafa, M. E.; Gadepalli, V. S.; Elmak, A. A.; Lee, W. R.; Rao, R. R.; Yadavalli, V. K. Large Area Micropatterning of Cells on Polydimethylsiloxane Surfaces. *J. Biol. Eng.* **2014**, *8*, 24.
(35) Yan, X.; Yao, J.; Lu, G.; Li, X.; Zhang, J.; Han, K.; Yang, B. Fabrication of Non-Close-Packed Arrays of Colloidal Spheres by Soft Lithography. *J. Am. Chem. Soc.* **2005**, *127* (21), 7688−7689.
(36) Lotito, V.; Zambelli, T. Pattern Detection in Colloidal Assembly: A Mosaic of Analysis Techniques. *Adv. Colloid Interface Sci.* **2020**, *284*, 102252.
(37) Raut, H. K.; Ganesh, V. A.; Nair, A. S.; Ramakrishna, S. Anti-Reflective Coatings: A Critical, in-Depth Review. *Energy Environ. Sci.* **2011**, *4* (10), 3779.
(38) Choy, T.. *Effective Medium Theory: Principles and Applications*; Oxford University Press, 2015.
(39) Fung, T. H.; Veeken, T.; Payne, D.; Veettil, B.; Polman, A.; Abbott, M. Application and Validity of the Effective Medium Approximation to the Optical Properties of Nano-Textured Silicon Coated with a Dielectric Layer. *Opt. Express* **2019**, *27* (26), 38645−38660.
(40) Lora Gonzalez, F.; Chan, L.; Berry, A.; Morse, D. E.; Gordon, M. J. Simple Colloidal Lithography Method to Fabricate Large-Area Moth-Eye Antireflective Structures on Si, Ge, and GaAs for IR Applications. *J. Vac. Sci. Technol. B* **2014**, *32* (5), 051213.
(41) Bushunov, A. A.; Tarabrin, M. K.; Lazarev, V. A. Review of Surface Modification Technologies for Mid-Infrared Antireflection Microstructures Fabrication. *Laser Photonics Rev.* **2021**, *15* (5), 2000202.
(42) Bartschmid, T.; Wendisch, F. J.; Farhadi, A.; Bourret, G. R. Recent Advances in Structuring and Patterning Silicon Nanowire Arrays for Engineering Light Absorption in Three Dimensions. *ACS Appl. Energy Mater.* **2022**, *5* (5), 5307−5317.
(43) Sahoo, K. C.; Lin, M.-K.; Chang, E.-Y.; Tinh, T. B.; Li, Y.; Huang, J.-H. Silicon Nitride Nanopillars and Nanocones Formed by Nickel Nanoclusters and Inductively Coupled Plasma Etching for Solar Cell Application. *Jpn. J. Appl. Phys.* **2009**, *48* (12R), 126508.
(44) Walde, S.; Hagedorn, S.; Coulon, P.-M.; Mogilatenko, A.; Netzel, C.; Weinrich, J.; Susilo, N.; Ziffer, E.; Matiwe, L.; Hartmann, C.; et al.et al. AlN Overgrowth of Nano-Pillar-Patterned Sapphire with Different Offcut Angle by Metalorganic Vapor Phase Epitaxy. *J. Cryst. Growth* **2020**, *531*, 125343.
(45) Cho, S. J.; An, T.; Lim, G. Three-Dimensionally Designed Anti-Reflective Silicon Surfaces for Perfect Absorption of Light. *Chem. Commun.* **2014**, *50* (99), 15710−15713.
(46) Bernhard, C. G.; Miller, W. H. A Corneal Nipple Pattern in Insect Compound Eyes. *Acta Physiol. Scand.* **1962**, *56* (3−4), 385−386.
(47) Chen, Y.-A.; Chen, I.-T.; Chang, C.-H. Increasing Etching Depth of Sapphire Nanostructures Using Multilayer Etching Mask. *J. Vac. Sci. Technol. B* **2019**, *37* (6), 061606.
(48) Ke, R.; Zhang, Y.; Zhou, Y. Study on Infrared Emissivity of Biomimetic Motheye Sapphire Single Crystal. *Optik* **2014**, *125* (23), 6991−6994.
(49) Liu, X.-Q.; Zhang, Y.-L.; Li, Q.-K.; Zheng, J.-X.; Lu, Y.-M.; Juodkazis, S.; Chen, Q.-D.; Sun, H.-B. Biomimetic Sapphire Windows Enabled by Inside-out Femtosecond Laser Deep-Scribing. *PhotoniX* **2022**, *3* (1), 1.
(50) Chien, K.-C.; Graff, N.; Djurdjanovic, D.; Chang, C.-H. In Situ Monitoring of Sapphire Nanostructure Etching Using Optical Emission Spectroscopy. *J. Vac. Sci. Technol. B* **2023**, *41* (6), 062807.
(51) Ravipati, S.; Shieh, J.; Ko, F.-H.; Yu, C.-C.; Chen, H.-L. Ultralow Reflection from A-Si Nanograss/Si Nanofrustum Double Layers. *Adv. Mater.* **2013**, *25* (12), 1724−1728.
(52) Verma, L. K.; Sakhuja, M.; Son, J.; Danner, A. J.; Yang, H.; Zeng, H. C.; Bhatia, C. S. Self-Cleaning and Antireflective Packaging Glass for Solar Modules. *Renew. Energy* **2011**, *36* (9), 2489−2493.
(53) Zhao, J.; Zhang, X.; Yonzon, C. R.; Haes, A. J.; Van Duyne, R. P. Localized Surface Plasmon Resonance Biosensors. *Future Med.* **2006**, *1* (2), 219−228.
(54) Dalby, M. J.; Riehle, M. O.; Sutherland, D. S.; Agheli, H.; Curtis, A. S. G. Fibroblast Response to a Controlled Nanoenvironment Produced by Colloidal Lithography. *J. Biomed. Mater. Res., Part A* **2004**, *69A* (2), 314−322.
(55) Dalby, M. J.; Riehle, M. O.; Sutherland, D. S.; Agheli, H.; Curtis, A. S. G. Changes in Fibroblast Morphology in Response to Nano-Columns Produced by Colloidal Lithography. *Biomaterials* **2004**, *25* (23), 5415−5422.
(56) Kuo, C. W.; Chueh, D.-Y.; Chen, P. Investigation of Size−Dependent Cell Adhesion on Nanostructured Interfaces. *J. Nanobiotechnol.* **2014**, *12* (1), 54.
(57) Niepel, M. S.; Fuhrmann, B.; Leipner, H. S.; Groth, T. Nanoscaled Surface Patterns Influence Adhesion and Growth of Human Dermal Fibroblasts. *Langmuir* **2013**, *29* (43), 13278−13290.
(58) Wang, P.-Y.; Bennetsen, D. T.; Foss, M.; Ameringer, T.; Thissen, H.; Kingshott, P. Modulation of Human Mesenchymal Stem Cell Behavior on Ordered Tantalum Nanotopographies Fabricated Using Colloidal Lithography and Glancing Angle Deposition. *ACS Appl. Mater. Interfaces* **2015**, *7* (8), 4979−4989.
(59) June, C. H.; O'connor, R. S.; Kawalekar, O. U.; Ghassemi, S.; Milone, M. C. CAR T Cell Immunotherapy for Human Cancer. *Science* **2018**, *359* (6382), 1361−1365.
(60) Rosenberg, S. A.; Restifo, N. P. Adoptive Cell Transfer as Personalized Immunotherapy for Human Cancer. *Science* **2015**, *348* (6230), 62−68.
(61) Hickey, J. W.; Vicente, F. P.; Howard, G. P.; Mao, H.-Q.; Schneck, J. P. Biologically Inspired Design of Nanoparticle Artificial Antigen-Presenting Cells for Immunomodulation. *Nano Lett.* **2017**, *17* (11), 7045−7054.
(62) Cheung, A. S.; Zhang, D. K. Y.; Koshy, S. T.; Mooney, D. J. Scaffolds That Mimic Antigen-Presenting Cells Enable Ex Vivo Expansion of Primary T Cells. *Nat. Biotechnol.* **2018**, *36* (2), 160−169.
(63) Dang, A. P.; De Leo, S.; Bogdanowicz, D. R.; Yuan, D. J.; Fernandes, S. M.; Brown, J. R.; Lu, H. H.; Kam, L. C. Enhanced Activation and Expansion of T Cells Using Mechanically Soft Elastomer Fibers. *Adv. Biosyst.* **2018**, *2* (2), 1700167.
(64) Hammink, R.; Weiden, J.; Voerman, D.; Popelier, C.; Eggermont, L. J.; Schluck, M.; Figdor, C. G.; Verdoes, M. Semiflexible Immunobrushes Induce Enhanced T Cell Activation and Expansion. *ACS Appl. Mater. Interfaces* **2021**, *13*, 16007−16018.


https://doi.org/10.1021/acsami.3c18554
*ACS Appl. Mater. Interfaces* 2024, 16, 17846−17856

(65) Fadel, T. R.; Sharp, F. A.; Vudattu, N.; Ragheb, R.; Garyu, J.; Kim, D.; Hong, E.; Li, N.; Haller, G. L.; Pfefferle, L. D.; et al.et al. A Carbon Nanotube−Polymer Composite for T-Cell Therapy. *Nat. Nanotechnol.* **2014**, *9* (8), 639−647.
(66) Pandey, A.; Iraqi, M.; Toledo, E.; Al-Kader Yassin, A.; Podvalni, E.; Naaz, S.; Pandit, J. J.; Martin, C. U.; Le Saux, G.; Porgador, A.; et al.et al. Elastic Microstructures: Combining Biochemical, Mechanical, and Topographical Cues for the Effective Activation and Proliferation of Cytotoxic T Cells. *ACS Appl. Mater. Interfaces* **2023**, *15* (26), 31103−31113.
(67) Hartmann, J.; Schüßler-Lenz, M.; Bondanza, A.; Buchholz, C. J. Clinical Development of CAR T Cells—Challenges and Opportunities in Translating Innovative Treatment Concepts. *EMBO Mol. Med.* **2017**, *9* (9), 1183−1197.
(68) Le Saux, G.; Bar-Hanin, N.; Edri, A.; Hadad, U.; Porgador, A.; Schvartzman, M. Nanoscale Mechanosensing of Natural Killer Cells is Revealed by Antigen-Functionalized Nanowires. *Adv. Mater.* **2019**, *31* (4), 1805954.
(69) Bhingardive, V.; Kossover, A.; Iraqi, M.; Khand, B.; Le Saux, G.; Porgador, A.; Schvartzman, M. Antibody-Functionalized Nanowires: A Tuner for the Activation of T Cells. *Nano Lett.* **2021**, *21*, 4241−4248.
(70) Bhingardive, V.; Edri, A.; Kossover, A.; Saux, G. L.; Khand, B.; Radinsky, O.; Iraqi, M.; Porgador, A.; Schvartzman, M. Nanowire Based Mechanostimulating Platform for Tunable Activation of Natural Killer Cells. *Adv. Funct. Mater.* **2021**, *31* (26), 2103063.
(71) Bhingardive, V.; Le Saux, G.; Edri, A.; Porgador, A.; Schvartzman, M. Nanowire Based Guidance of the Morphology and Cytotoxic Activity of Natural Killer Cells. *Small* **2021**, *17* (14), 2007347.
(72) Pokroy, B.; Kang, S. H.; Mahadevan, L.; Aizenberg, J. Self-Organization of a Mesoscale Bristle into Ordered, Hierarchical Helical Assemblies. *Science* **2009**, *323* (5911), 237−240.
(73) Huse, M. Mechanical Forces in the Immune System. *Nat. Rev. Immunol.* **2017**, *17* (11), 679−690.
(74) Aramesh, M.; Stoycheva, D.; Sandu, I.; Ihle, S. J.; Zünd, T.; Shiu, J.-Y.; Forró, C.; Asghari, M.; Bernero, M.; Lickert, S.; et al.etal. Nanoconfinement of Microvilli Alters Gene Expression and Boosts T Cell Activation. *Proc. Natl. Acad. Sci. U. S. A.* **2021**, *118* (40), No. e2107535118.
(75) Tan, J. L.; Tien, J.; Pirone, D. M.; Gray, D. S.; Bhadriraju, K.; Chen, C. S. Cells Lying on a Bed of Microneedles: An Approach to Isolate Mechanical Force. *Proc. Natl. Acad. Sci. U. S. A.* **2003**, *100* (4), 1484−1489.
(76) Bashour, K. T.; Gondarenko, A.; Chen, H.; Shen, K.; Liu, X.; Huse, M.; Hone, J. C.; Kam, L. C. CD28 and CD3 Have Complementary Roles in T-Cell Traction Forces. *Proc. Natl. Acad. Sci. U. S. A.* **2014**, *111* (6), 2241−2246.
(77) Acharya, S.; Hill, J. P.; Ariga, K. Soft Langmuir−Blodgett Technique for Hard Nanomaterials. *Adv. Mater.* **2009**, *21* (29), 2959−2981.


https://doi.org/10.1021/acsami.3c18554
*ACS Appl. Mater. Interfaces* 2024, 16, 17846−17856